Hindawi Publishing Corporation
Journal of Nanomaterials
Volume 2013, Article ID 426983, 11 pages
http://dx.doi.org/10.1155/2013/426983

Research Article

Synthesis of Polypyrrole Inverse Opal in [bmim]PF_6^- Containing Acetonitrile and the Application of the Inverse Opal in Cell Prototype

Wei Yan,[1] Qi-Qi Dong,[1] Li-Ning Sun,[1] Wei Deng,[1] and Shaoping Wu[2]

[1] *Nano-Science and Technology Research Center, Shanghai University, Shanghai 200444, China*
[2] *College of Physical Science and Technology, Huazhong Normal University, Wuhan 430079, China*

Correspondence should be addressed to Wei Yan; yveayan@shu.edu.cn and Wei Deng; wdeng@shu.edu.cn

Received 19 November 2012; Accepted 6 December 2012

Academic Editor: Yongfeng Luo

Most primary cells use Zn or Li as the anode, a metallic oxide as the cathode, and an acidic or alkaline solution or moist past as the electrolytic solution. In this paper, highly ordered polypyrrole (PPy) inverse opals have been successfully synthesized in the acetonitrile solution containing [bmim]PF_6. PPy films were prepared under the same experimental conditions. Cyclic voltammograms of the PPy film and the PPy inverse opal in neutral phosphate buffer solution (PBS) were recorded. X-ray photoelectron spectroscopy technique was used to investigate the structural surface of the PPy films and the PPy inverse opals. It is found that the PF_6^- anions kept dedoping from the PPy films during the potential scanning process, resulting in the electrochemical inactivity. Although PF_6^- anions also kept dedoping from the PPy inverse opals, the PO_4^{3-} anions from PBS could dope into the inverse opal, explaining why the PPy inverse opals kept their electrochemical activity. An environmental friendly cell prototype was constructed, using the PPy inverse opal as the anode. The electrolytes in both the cathodic and anodic half-cells were neutral PBSs. The open-circuit potential of the cell prototype reached 0.487 V and showed a stable output over several hundred hours.

1. Introduction

Polypyrrole (PPy) was first reported by an Italian group, Dall'Olio et al. in 1961. Since then, PPy has generated significant interest for the last four decades, because of its high conductivity and environmental stability. PPy has found use in a wide range of applications, including chemical and biological sensors, light emitting diodes, electromagnetic interference shielding, and advanced battery systems [1, 2]. There are many methods of preparing electroconducting polymers from monomer solutions. Among them, electropolymerization is the preferred general method because of its simplicity and reproducibility. Moreover, electropolymerization has merits that new properties can be easily obtained by use of various supporting electrolytes, and the film thickness also can be easily controlled by regulating the amount of charge passed [2]. Room temperature ionic liquids (ILs), which are composed of unsymmetrically substituted nitrogen-containing cations (imidazole, pyrrolidine, pyridine, etc.) with inorganic anions (Cl^-, PF_6^-, BF_4^-, etc.), have many unique physicochemical properties, such as high thermal stability, negligible vapor pressure, good electrochemical stability and conductivity at room temperature [3]. ILs have now been used as new types of dopants in electroconducting polymer synthesis. Several groups have prepared PPy films doped with different ILs via electropolymerization method [4–8]. Though the properties of ILs-doped PPy films depend on the polymerization conditions and the nature of ILs [6], the electrochemical stability and conductivity of PPy films were reported to have been greatly improved by ILs.

Recently, three-dimensional ordered macroporous (3DOM) materials, with interconnected macropores (the so-called "inverse opals"), have attracted increasing attention due to their well-designed structures, huge surface area, and unique properties [9–13]. Now, several methods, such as nanomachining, photolithography, and three-dimension (3D) holography, have been developed for the synthesis of 3D periodically modulated dielectric materials. Among them, self-assembly has been demonstrated as a facile and

inexpensive way to produce 3D photonic crystals. Several methods concerning the synthesis of inverse opals have been developed, and, among them, using self-assembled colloid crystals as the templates has stood out in the inverse opal synthesis [14–18]. The void spaces of colloid crystals templates can be filled with other materials and the spheres can be subsequently removed. Among these templates, silica spheres are ideal candidate templates since they can be obtained conveniently in desired sizes. Furthermore, commercial silica spheres are available now and can be simply removed by dissolution with an aqueous hydrofluoric acid solution. We have used SiO_2 colloid crystals for the fabrication of gold inverse opals and found that it showed excellent performance in the antibody and antigen detection [19].

Inverse opals based on different conducting polymers, such as PPy [10, 20], polyaniline (PAni) [21], polyphenylenevinylene (PPV), and polythiophene (PTh) [9] have been prepared by electrochemical polymerizing the corresponding monomer in the interstitial voids of the colloid crystal template. PPy is desirable as inverse opal due to its ease of synthesis, inexpensive monomer, stability in ambient conditions, and relatively high levels of electrical conductivity. The original interest for preparing inverse opals with conducting polymers originated from the motivation to obtain photonic band gap crystals of conjugated polymers, whose refractive index can be easily tuned [22–24]. Now, considerable research interest is focused on the potential applications of electroconducting polymer inverse opals for other purposes, by exploiting the advantages provided by the highly ordered porous structure of electroconducting polymer inverse opal [22].

Herein, a kind of PPy inverse opal was synthesized through electropolymerization in the acetonitrile solution. A self-assembled SiO_2 colloid crystal was used as the sacrificial template. The viscosity of $[bmim]PF_6$ is so high that it could not go into the voids of the colloid crystal template. The electropolymerization had to be carried out in a acetonitrile solution containing both $[bmim]PF_6$ and pyrrole monomer. During the electropolymerization, no typical doping and dedoping peaks were observed, resulting from the acidic nature of $[bmim]^+$.

Electrodeposition was usually used to prepare electroconducting polymer inverse opals, applying a constant current or potential for an appropriate time. However, we found that highly ordered PPy inverse opals could also be obtained by cyclic voltammetric method. As the counterpart, PPy films were prepared under the same experimental conditions. Cyclic voltammograms of PPy film and PPy inverse opal in neutral phosphate buffer solution (PBS) were recorded. After hundreds of potential scanning cycles, the PPy film totally lost its electrochemical activity, while the redox peaks could still be observed on the cyclic voltammgram of the PPy inverse opal. X-ray photoelectron spectroscopy (XPS) technique was used to investigate the structure change of the PPy film and the PPy inverse opal before and after the cyclic voltammetry. It is found that during the potential scanning, the PF_6^- anions kept dedoping from the PPy film, that is the reason why the PPy film lost its electrochemical activity after hundreds of potential scanning cycles. Although the PF_6^- anions also kept dedoping from the PPy inverse opal, the PO_4^{3-} anions from the buffer solution would insert into the PPy backbone during the potential scanning, explaining why the redox peaks could be observed.

A cell prototype which can operate in a physiological buffer was constructed. The open-circuit potential (OCP) of the cell reached 0.487 V. The cell prototype showed stable output over several hundred hours.

2. Experimental

2.1. Preparation of SiO_2 Colloid Crystal Template. The monodisperse silica spheres with the diameters of 0.50 mm were obtained from Alfa Aesar. The gold substrates, supplied by the 55th institute of China electronic group, were prepared by sputtering a 200 nm thick gold top layer onto the quartz wafers. Before use, the substrates were thoroughly rinsed with acetone, ethanol, and water and then vertically immersed into an ethanol suspension containing 0.09 g/mL monodispersed SiO_2 spheres. This apparatus was covered with a 1000 mL beaker and kept in a temperature-controlled oven at 40°C for 48 hours for the self-assembling of SiO_2 spheres.

2.2. Preparations of the PPy Films and the PPy Inverse Opals. $[bmim]PF_6$ was commercial obtained. Pyrrole monomer was distilled under reduced pressure before use. Electropolymerization was carried out with a cyclic potential scanning sweep method in a three-electrode configuration on a CHI660C electrochemical workstation (Chenhua, China). A platinum wire served as the counterelectrode, and the reference electrode was made according to [25], immersing a Ag/AgCl wire into a 1 M solution of $AgNO_3$ in acetonitrile into 450 μL $[bmim]PF_6$. Due to volatility of acetonitrile, the three-electrode configuration was airtight. The potential was swept between −0.5 and 0.65 V versus Ag/AgCl reference electrode at a sweep rate of 0.1 V/s. A gold substrate was used as the working electrode for the synthesis of the PPy film, and a gold substrate covered by a SiO_2 colloid crystal template was used as the working electrode for the preparation of the PPy inverse opal. After 250 potential scanning cycles, a black film was formed on the gold substrate. The PPy inverse opal was obtained after the SiO_2 template was removed by 10% HF solution. The morphology of the SiO_2 colloid crystal template and the PPy inverse opal were verified by field-emission scanning electron microscope (FESEM, JEOL JEM-2010F).

2.3. XPS Analysis. The XPS spectra were acquired by using Al Kα radiation (1486.6 eV) through a Perkin-Elmer PHI 5000C ESCA system at a base pressure of 1×10^{-9} Torr equipped an electronic neutralization gun to eliminate the charge effect on the sample surface. The sample was firstly pressed to a 1×13 mm disc and fixed to the sample holder, it was then degassed in the pretreatment chamber for 2 h. After that, it was removed to the test chamber for XPS study. All binding energy values were calibrated by using the value of contaminant carbon (C1s = 284.6 eV) as a reference. The surface composition of doped polypyrrole samples was

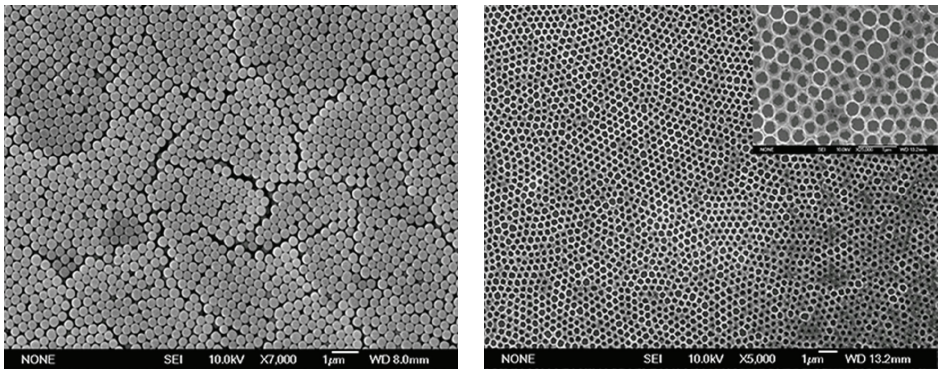

(a) (b)

Figure 1: The SEM image of the SiO_2 colloid crystal template prepared by vertical deposition (a); the SEM image of a PPy inverse opal (b).

calculated from the areas of the Cls, Ols, Nls, F1s, P2p3, Si2p3, and Na1s photoelectron peaks.

Eight samples were prepared for the XPS analysis. Sample I is the prepared PPy film, sample II was prepared by soaking sample I into a 10% HF solution for about 30 s. Sample III is the prepared PPy inverse opal, and sample IV was obtained before the SiO_2 template of sample III was removed.

Cyclic voltammetry were conducted in PBS of pH 7.0 using a three-electrode configuration. The samples served as the working electrode. A Pt wire and a SCE were used as the counterelectrode and reference electrode, separately. The potential scanned from −1.0 to 0.70 V (versus SCE) with the scanning rate of 0.1 V/s until the current did not change anymore. The samples were then taken out of the PBS solution, washed with deionized water and dried in air. The new samples after the cyclic voltammetry were the other four samples for XPS analysis, which denoted as sample I/CV, sample II/CV, sample III/CV, and sample IV/CV, separately.

2.4. Construction of the Cell Prototype. A cell prototype was constructed. The anode of the cell was a PPy inverse opal modified gold substrate. The geometric area of the PPy inverse opaline film on the gold substrate was controlled by insulating tape, and was determined to be 0.35 cm^2. The cathode was a platinum plate (2 mm × 6 mm). The electrolytes in both the cathodic and anodic half-cells were PBS of pH 7.0. A KCl salt bridge was used to connect the two half-cells. The performance of the cell was evaluated at room temperature.

3. Results and Discussion

3.1. Characterization Results of the SiO_2 Colloid Crystal Template and the PPy Inverse Opal. A number of self-assembly techniques, including gravitational sedimentation, vertical deposition, membrane filtration, emulsion crystallization, and Langmuir-Blogett (LB) method, have been involved in the fabrications of photonic crystals [26, 27]. Vertical deposition, which takes use of the evaporation-induced self-assembly driven by capillary forces, can produce superior quality colloid crystals. The efficiency of vertical deposition relies on the balance between solvent evaporation and particle sedimentation. Thus, temperature and particle concentration played very important roles in the self-assembly of well-ordered optical crystals via vertical deposition [28].

Figure 1(a) shows the SEM image of the SiO_2 colloid crystal template on a gold substrate. It can be seen that the template consisted of well-ordered 3D arrays of SiO_2 spheres and exhibited a face-centered-cubic structure with (111) planes parallel to the substrate. Electropolymerization was carried out with a cyclic voltammetric method in a three-electrode configuration.

Though cyclic voltammetry technique is normally used in electropolymerization of electroconducting polymers, the syntheses of electroconducting film inverse opals were usually carried out by electrodeposition in monomer-containing aqueous solutions, applying a constant current or potential for an appropriate time [29]. There has been no report on preparing electroconducting film inverse opals through cyclic voltammetry method, and here we tried to prepare PPy inverse opals via cyclic voltammetry technique. Though $[bmim]PF_6$ has already shown to be excellent media for the electrochemical synthesis of PPy films [1], the viscosity of $[bmim]PF_6$ is so high that it could not penetrate into the voids of SiO_2 template. Finally, the electropolymerization was carried out in an acetonitrile solution containing 0.1 M pyrrole monomer and 0.1 M $[bmim]PF_6$. After the SiO_2 template was removed, highly ordered PPy inverse opal was obtained on the gold substrate.

Figure 1(b) displays the SEM image of the PPy inverse opal on a gold substrate. We found that a highly regular PPy inverse opal had been obtained by cyclic voltammetric technique. It can be seen from the enlarged image (the insert of Figure 2(b)) that the inverse opal is of one layer thickness.

3.2. Electropolymerization Processes of the PPy Film and the PPy Inverse Opal. Figure 2(a) shows the cyclic voltammogram of the first twenty cycles in the course of electropolymerization of pyrrole on a gold substrate in the acetonitrile solution containing 0.1 M pyrrole and 0.1 M $[bmim]PF_6$. The potential was scanned from −0.5 V to 0.65 V with a scanning rate of 0.1 V/s. With each successive scan, the cathodic and anodic wave currents increased, suggesting the continuous

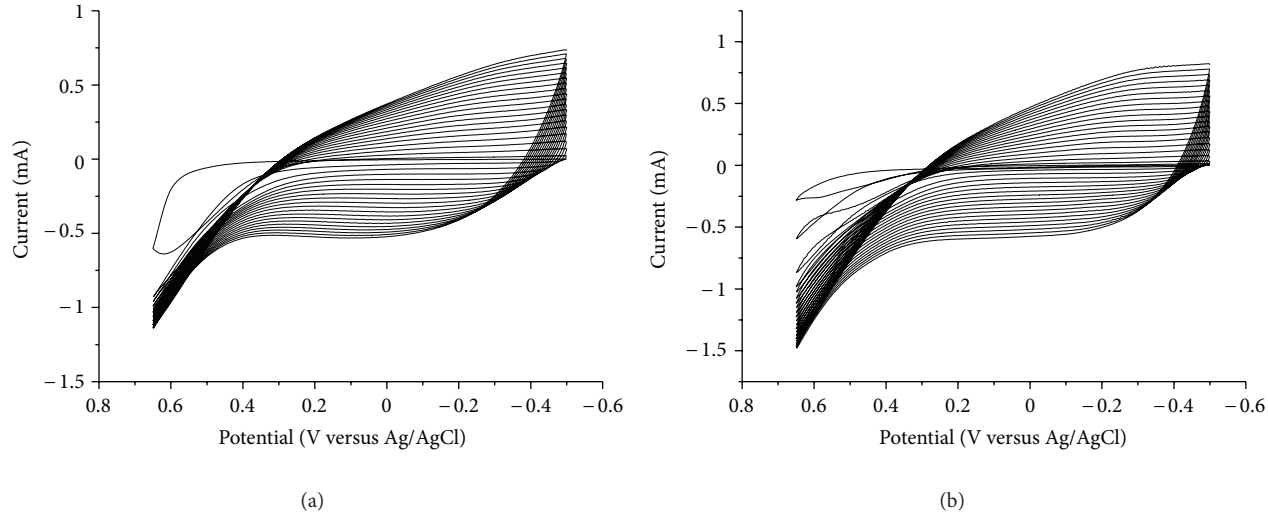

Figure 2: Cyclic voltammogram of the first twenty cycles in the course of electropolymerization of pyrrole in acetonitrile containing 0.1 M pyrrole and 0.1 M [bmim]PF_6 at 0.1 V/s between −0.5 and 0.65 V versus the homemade Ag/AgCl reference electrode on a gold substrate (a) and on a gold substrate covered by SiO_2 colloid crystal template (b).

deposition of PPy films on the gold substrate. Figure 2(b) shows the cyclic voltammogram of the first twenty cycles in the course of electropolymerization of pyrrole on a gold substrate covered by a SiO_2 colloid crystal template. Both the cathodic the anodic wave currents increased cycle by cycle, indicating the continuous deposition of PPy films on the SiO_2 colloid crystal template.

Normally, a pair of sharp redox peaks could be observed during the cyclic voltammetric electropolymerization process of pyrrole. In both Figures 2(a) and 2(b), however, no peaks but broad waves emerged in the potential scanning range. Zhou et al. have done a series of researches on the electropolymerization of pyrrole in acetonitrile solutions [27, 30–33] and gave a detailed statement on the electropolymerization of pyrrole monomer in acetonitrile solutions [31]. In the electropolymerization process, there exists an intermediate, which was structurally confirmed as 2,2′-(2,5-pyrrolidinediyl)dipyrrole (IV). If the concentration of IVs is too high, the coupling mainly takes place between $IV^{(2).+}$, producing nonconducting polymer and passivating the electrode. Zhou et al. found that the concentration of IV depends on the switching potential during the scan as well as the acidity of the solution. More IVs would be produced at higher potential and higher acidity. The pKa value of the $[bmim]^+$ was found to be in the range of 21–24 in dimethyl sulfoxide (DMSO) and H_2O [34], which reveals the acidic nature of $[bmim]^+$. There is always some water in acetonitrile, and the addition of [bmim]PF_6 into the water-containing acetonitrile had increased the acidity of the acetonitrile solution. During our experiment, the potentiodynamic growth of PPy could be observed when the potential was scanned from −0.5 to 0.65 V. If the positive switching potential increased to 0.75 V, passivation would happen, suggesting that there were too much IVs generated. Zhou et al. also found that when the positive switching potential was low, passivation of electrode could also be observed. The concentration of Py^+ was very low at low potential, and the reactions involving $IV^{(2).+}$, were still determinative, resulting in the passivaton of either electrode. During our experiment, we also found that if the positive switching potential was lower than 0.58 V, the growth of PPy film could not be observed due to the low concentration of Py^+.

The PPy film could not grow when the positive switching potential was higher than 0.75 V or lower than 0.58V, indicating that the coupling reaction mainly took place between $IV^{(2).+}$, and Py^+. Zhou et al. found that no sharp redox peaks but wide waves were observed during the electropolymerization of PPy when the coupling reaction took place between $IV^{(2).+}$, and Py^+. In our experiments, also only wide waves were observed (Figures 2(a) and 2(b)). In both Figures 2(a) and 2(b), a large anodic peak could be observed on the first cycle during the electropolymerization. This anodic peak points out the anodic oxidation of pyrrole monomer on the substrate and the formation of PPy film. The anodic peak on the gold substrate (Figure 2(a)) is much larger than that on the gold substrate covered with a SiO_2 colloid crystal template (Figure 2(b)), which might be attributed to the fact that the real area of gold substrate is larger than that of the gold substrate covered with a SiO_2 colloid crystal template.

3.3. Cyclic Voltammograms of the PPy Film and the PPy Inverse Opal in 0.1 M PBS of pH 7.0. The electrochemical properties of the PPy film and the PPy inverse opal were characterized by cyclic voltammetry. Figure 3(a) shows the cyclic voltammogram of the first ten circles obtained at the PPy film modified gold substrate (PPy film/Au) in 0.1 M PBS of pH 7.0 scanning from −1.0 to 0.7 V. A pair of redox peaks was observed. The redox peaks correspond to the doping and dedoping of counteranions. With each successive scan, the currents of the redox peaks decreased. Eventually, all the reduction and oxidation peaks disappeared after hundreds of

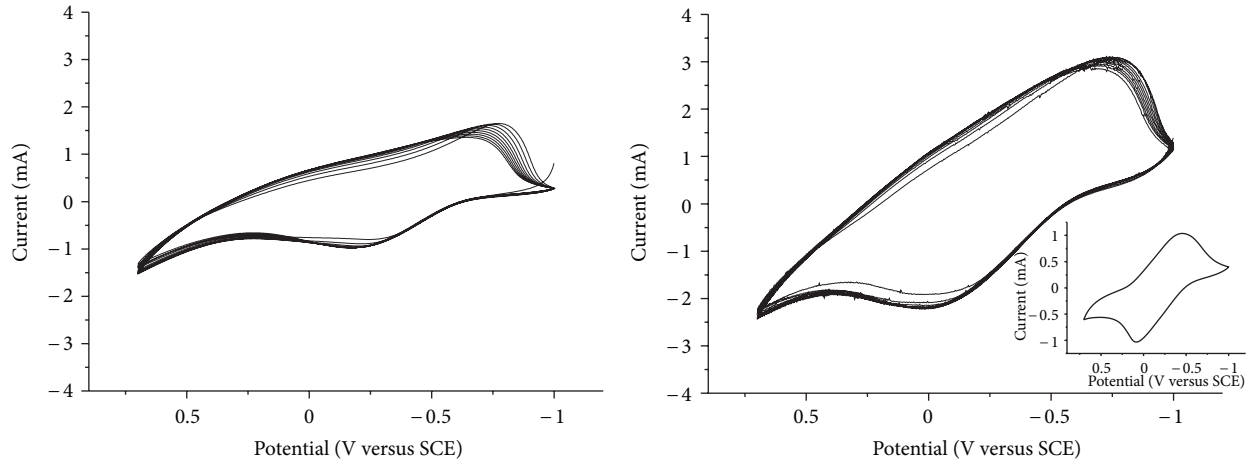

Figure 3: (a) Cyclic voltammogram of the first ten cycles obtained at the PPy film/Au in 0.1 M PBS of pH 7.0 scanning from −1.0 to 0.7 V at the scanning rate of 0.1 V/s; (b) cyclic voltammogram of the first ten cycles obtained at PPy inverse opal/Au in 0.1 M PBS of pH 7.0 scanning from −1.0 to 0.7 V at the scanning rate of 0.1 V/s (insert is the cyclic voltammogram obtained at the PPy inverse opal/Au scanning from −1.0 to 0.7 V after equilibrium was reached).

potential scanning cycles (not shown), indicating that there were almost no counteranions in the PPy film any more.

Figure 3(b) shows the cyclic voltammogram of the first ten circles obtained at the PPy inverse opal modified gold substrate (PPy inverse opal/Au) in 0.1 M PBS of pH 7.0 scanning from −1.0 to 0.7 V. An oxidation peak at −0.12 V and a reduction peak at −0.84 V were observed on the line. The oxidation peak corresponds to the doping of counteranions, and the reduction peak corresponds to the dedoping of counteranions. Although the redox peak currents decreased with each successive scan, the redox peaks could still be observed after thousands of scanning cycles when equilibrium was reached (insert of Figure 3(b)). The potential of oxidation peak shifted from −0.12 V to 0.12 V, and the potential of the reduction peak shifted from −0.80 V to −0.45 V.

3.4. XPS Analysis. To elucidate the structural change of PPy film and PPy inverse opal before and after cyclic voltammetry in neutral PBS solution, XPS was used to determine the surface composition of the electroconducting polymer. The XPS spectra were acquired by using Al Kα radiation (1486.6 eV) through a Perkin-Elmer PHI 5000C ESCA system. All binding energy values were calibrated by using the value of contaminant carbon (C_{1S} = 284.6 eV) as a reference [35]. In the XPS spectra of all the eight samples, the main C1s, N1s, O1s, F1s, P2p3, and Si2p3 peak were located at ca. 290 eV, 406 eV, 537 ev, 692 eV, 142 eV, and 96 eV, separately. Figure 4 shows the element atomic concentration percentages of C1s, N1s, O1s, F1s, P2p3, and Si2p3 on the samples surface. The element atomic concentration percentages were obtained from the integrated area under the principal peaks. The inserts in the Figure 4 display the N1s XPS core level spectra of the samples. The N1s signal originates from the nitrogen of the pyrrole rings of the polymer backbone because of lack of nitrogen in the dopants used.

Figure 4(a) presents the element atomic concentration percentages of C1s, N1s, O1s, F1s, P2p3, and Si2p3 at the surface of sample I (the PPy film). The atomic concentration ratio of P2p3 : N1s and F1s : N1s was 0.27 and 1.45, separately. Figure 4(b) shows atomic concentration percentages of the elements contributing to the sample I/CV. The atomic concentration ratio value of P2p3 : N1s at the surface of sample I decreased from 0.27 to 0.04 after the cyclic voltammetry, and the value of F1s : N1s decreased from 1.45 to 0.05. The values of P2p3 : N1s and F1s : N1s both decreased greatly after the cyclic voltammetry, indicating that the PF_6^- anions kept dedoping from the PPy film during the potential scanning process.

The insert in Figures 4(a) and 4(b) shows the N1s XPS core level spectrum of the sample I and the sample I/CV, respectively. The N1s spectra clearly indicate the existence of three inequivalent nitrogen heteroatoms either in the sample I or in the sample I/CV. In the insert of Figure 4(a), the peak I is attributed to nitrogen that is not influenced by the presence of any anions. The ratio of peak I to the total N1s peak area is 56.8%. The peak II shifting by 1.8 eV with respect to the main nitrogen feature is attributed to nitrogen interacting with the PF_6^- anions. The ratio of peak II to the total N1s peak area is 26.7%, indicating that the PPy film was consisted of the normally accepted structure containing about one PF_6^- anion per four pyrrole monomers. The ratio of peak III to the total N1s peak area is 8.3%. It should be noted oxygen was detected in all the eight samples by XPS. The peak III may be assigned to the interaction of nitrogen with some oxygen containing anions, such as hydroxyl groups. In the insert of Figure 4(b), the ratio of peak II to the total N1s peak area decreased from 26.7% to 4.7% after the cyclic voltammetry for the dedoping of PF_6^- anions. The ratio of peak I, however, increased from

56.8% to 86.6%. The ratio of the peak III did not change much after the cyclic voltammetry. From the analysis of the XPS spectra of the sample I and sample I/CV, it is found that the PPy film almost lost all its PF_6^- anions after the cyclic voltammetry. That is the reason why the redox peaks of the PPy film disappeared after hundreds of potential scanning cycles in PBS of pH 7.0.

Figure 4(c) presents the element atomic concentration percentages of the elements at the surface of sample II (the PPy film immersed into 10% HF solution for 30 s). The atomic concentration ratio of P2p3 : N1s and F1s : N1s of sample II was 0.18 and 0.51, respectively. As the doped PF_6^- anions might decompose during the incubation in the 10% HF solution, the atomic ratios of P2p3 : N1s and F1s : N1s of sample II are much smaller than that of sample I. Figure 4(d) displays element atomic concentration percentages of the elements at the surface of sample II/CV. The atomic concentration ratio of P2p3 : N1s and F1s : N1s of sample II was 0.023 and 0.4, respectively. The reduction of the atomic concentration ratios of P2p3 : N1s and F1s : N1s can be ascribed to the dedoping of PF_6^- anions from the sample II during the potential scanning process.

The insert in Figures 4(c) and 4(d) shows the N1s XPS core level spectrum of the sample II and sample II/CV, respectively. The N1s spectra indicate clearly the existence of two inequivalent nitrogen heteroatoms in both sample II and sample II/CV. In the insert of Figure 4(c), the peak I is attributed to nitrogen that is not influenced by the presence of any anions. The ratio of peak I to the total N1s peak area is 81.6%. The peak II shifting by 1.8 eV with respect to the main nitrogen feature is attributed to the electrostatic interaction with the PF_6^- anions. The ratio of peak II to the total N1s peak area is 18.4%. As the doped PF_6^- anions decomposed during the incubation in 10% HF solution, the ratio of peak II of sample II is lower than that of sample I, while the ratio of peak I is higher. In the N1s XPS core level spectrums of the sample II and sample II/CV, peak III, which can be assigned to the interaction of nitrogen with hydroxyl groups, is not observed. The hydroxyl groups at the surface of the samples might have been removed by 10% HF solution. In the insert of Figure 4(b), the ratio of peak II to the total N1s peak area decreases from 18.4% to 2.4% for the dedoping of PF_6^- anions. The ratio of peak I, however, increases from 81.6% to 97.6%. From the analysis of the XPS spectra of the sample II and sample II/CV, it is found that almost all the PF_6^- anions have dedoped from the sample II after hundreds of potential scanning cycles.

Figure 4(e) presents the element atomic concentration percentages of the elements at the surface of sample III (the PPy inverse opal). As the decomposition of PF_6^- anions resulting from the 10% HF solution, the atomic concentration ratios of P2p3 : N1s and F1s : N1s of sample III were only 0.12 and 0.16, separately. Figure 4(f) displays element atomic concentration percentages of the elements at the surface of sample III/CV. The atomic concentration ratio of P2p3 : N1s and F1s : N1s of sample III/CV was 0.12 and 0.04, respectively. Same with the sample I and sample II, the PF_6^- anions kept dedoping from the electroconducting polymer, explaining the reason why the value of F1s : N1s was close to zero after thousands of scanning cycles. The value of P2p3 : N1s, however, almost did not change, indicating that there were still many phosphorous containing groups in the PPy inverse opal when the equilibrium reached. As the PF_6^- anions had dedoped from the PPy inverse opal, we think that it is the PO_4^{3-} anions from the PBS that doped into the PPy inverse opal during the potential scanning process, leading to the constant ratio value of P2p3 : N1s.

As PPy was electropolymerized on the gold substrate covered with a SiO_2 colloid crystal template during the synthesis of PPy inverse opals, it is very hard to know how many inequivalent nitrogen heteroatoms existed in the samples through the N1s XPS core level spectra. However, the variations of the atomic concentration ratios of P2p3 : N1s and F1s : N1s suggested the dedoping of PF_6^- anions and the doping of PO_4^{3-} anions during the cyclic voltammetry process. The substitution of PF_6^- anions by PO_4^{3-} anions explains well why redox peaks were still observed on the cyclic voltammetric curves of the PPy inverse opal after thousands of potential scanning cycles. As the PF_6^- anions in the PPy inverse opal have been replaced by PO_4^{3-} anions, the redox peak potentials both shifted after the equilibrium reached.

Figure 4(g) presents the element atomic concentration percentages of the elements at the surface of the sample IV (PPy inverse opal before the SiO_2 was removed). As there was no decomposition of PF_6^- anions, the atomic concentration ratios of P2p3 : N1s (0.18) and F1s : N1s (1.35) of the sample IV were higher than that of the sample III. From value of P2p3 : N1s, it can be seen that the electroconducting polymer was consisted of the structure containing about one PF_6^- anion per five pyrrole monomers when the electropolymerization took place on the gold substrate covered with a SiO_2 colloid crystal template. Figure 4(f) displays element atomic concentration percentages of the elements at the surface of the sample IV/CV. The atomic concentration ratio of P2p3 : N1s and F1s : N1s of the sample IV/CV was 0.21 and 0.98, respectively. The dedoping of PF_6^- anions led to the reduction in the F1s : N1s value after the cyclic voltammetry. The ratio of P2p3 : N1s, however, increased from 0.18 to 0.21, indicating that a great number of PO_4^{3-} anions from the electrolyte have doped into the sample IV during the potential scanning process.

From the analysis of Figures 4(a), 4(b), 4(c), and 4(d), it can be seen that the incubation of the film in 10% HF solution would lead to the decomposition of PF_6^- anions. The decomposition of the PF_6^- anions, however, did not change the electrochemical behavior of PPy films in neutral PBS. The doped PF_6^- anions in the PPy films kept dedoping, resulting in the electrochemical inactivity after hundreds of potential scanning cycles.

From the analysis of Figures 4(d), 4(e), 4(g), and 4(f), it can be seen that no matter the SiO_2 template was removed or not, the electrochemical behavior of PPy film inverse opals was different with that of the PPy films. Although PF_6^- anions also kept dedoping from the PPy inverse opals, the PO_4^{3-} anions from PBS could dope into the inverse opal. When the SiO_2 template was removed, the PPy inverse opal

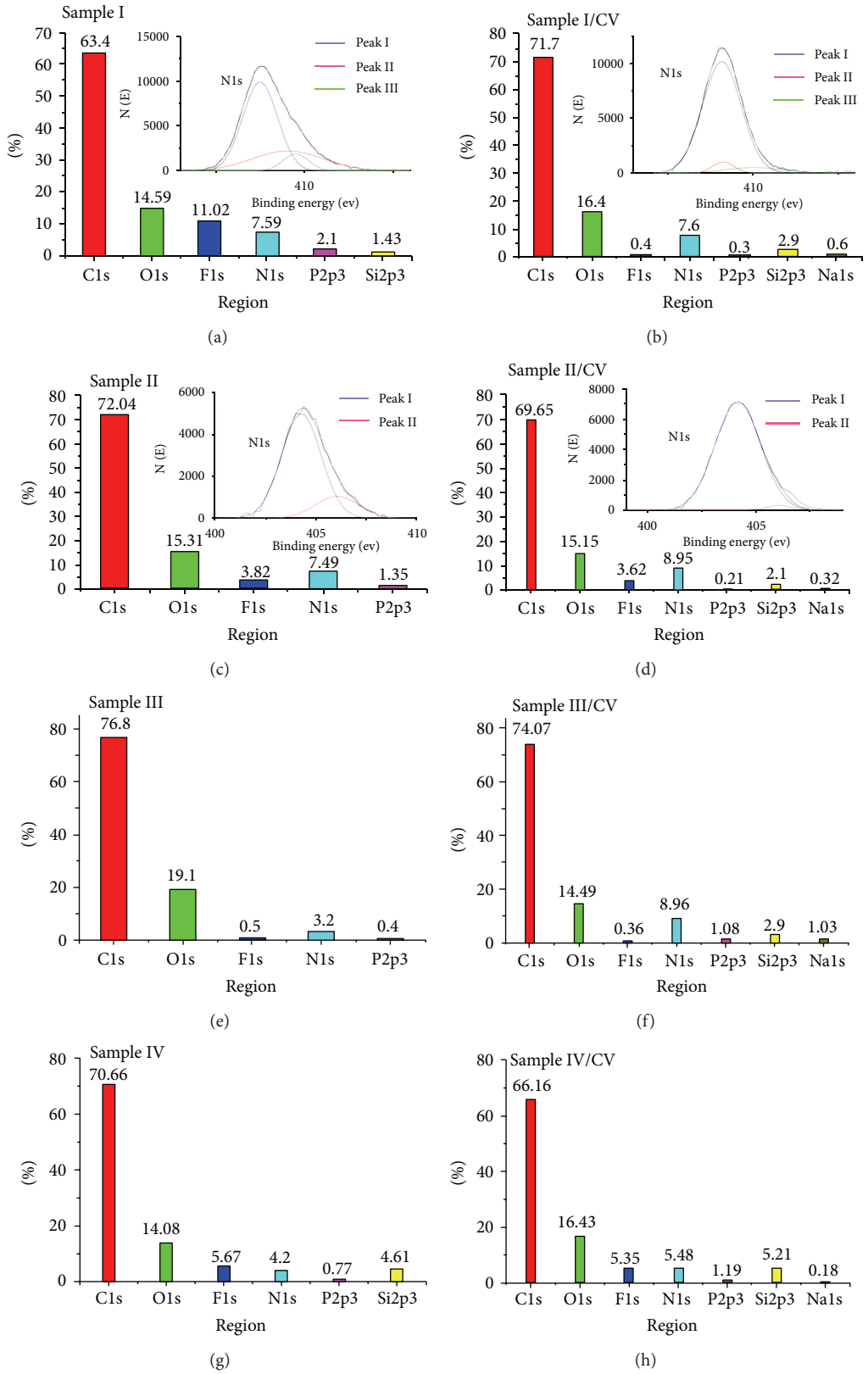

Figure 4: Element atomic concentration percentages of C1s, N1s, O1s, F1s, P2p3, and Si2p3 at the surface of (a) sample I, (b) sample I/CV, (c) sample II, (d) sample II/CV, (e) sample III, (f) sample III/CV, (g) sample IV, and (h) sample IV/CV (insert is N1s XPS core level spectrum of the corresponding sample).

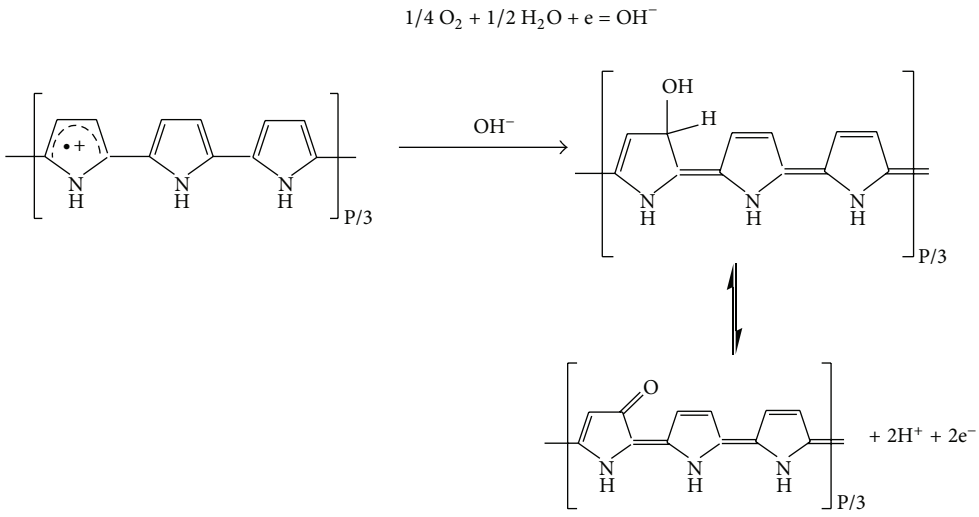

Scheme 1

did not have the macroporous structure. The observations indicated that it was not the macroporous structure that resulted in the different electrochemical behavior of PPy film and PPy inverse opal in neutral PBS. The different electrochemical behavior might be ascribed to the different backbone structure of PPy film and PPy inverse opal.

3.5. Construction of a Cell Prototype Operating in a Physiological Buffer Based on PPy Inverse Opals. A cell prototype which can operate in a physiological buffer was developed as Figure 5. The anode of the cell is the PPy inverse opal/Au, and the cathode is a platinum plate (2 mm × 6 mm). The electrolytes in both the cathodic and anodic half-cells were PBS of pH 7.0. A KCl salt bridge was used to connect the two half-cells. This cell prototype holds tremendous potential for development into wide use. Conducting polymers are often used as cathodes coupled with metal anodes in batteries with nonaqueous electrolytes. Here, the PPy inverse opal was used as the anode coupled with a Pt cathode with neutral aqueous electrolyte, which holds the potential development into use in biocell in the future.

The OCP of the cathodic and anodic electrodes were investigated with three-electrode system, where SCE and Pt wire served as the reference and counterelectrode respectively. It can be observed from Figure 6(a) that the OCP of the Pt plate electrode in 0.1 M PBS of pH 7.0 kept at c.a. 0.29 V in the air (curve b). The OCP of the PPy inverse opal/Au maintained at −0.32 V in 0.1 M PBS of pH 7.0 when the buffer solution was saturated with N_2 (curve a). The OCP of the cell was about 0.487 V when the air in the anodic half-cell was thoroughly removed by bubbling nitrogen.

Beck and Michaelis in an earlier study indicated that electrochemically obtained films of PPy prepared in the absence of air or H_2O are reactive to O_2 [36]. In our research, we found that the PPy inverse opal/Au should be immediately immersed into PBS and used as the anode of the cell prototype after it was prepared. If the PPy inverse opal/Au was left in air more than 1 hour before it was used to construct the cell prototype, the OCP of the cell would be close to zero.

Beck et al. have done a research on the stability of PPy films in aqueous buffer solution [36, 37]. He found that the PPy films prepared in acetonitrile solution still remained radical cationic centers after electropolymerization. The radical cationic centers could be attacked by the nucleophilic reagent (i.e., OH^-) in aqueous solution, leading to the formation of a quinoid structure and release of electrons [37] (see Scheme 1).

The cathode and anode reactions of the cell prototype are separately

A plot of the stability of the cell output, evaluated by measuring the power density with 200 KΩ load, is presented in Figure 6(b). The power density was normalized by the geometry surface area of the anode. The power density decreased to ca. 25% (0.41 μW/cm^2) of the initial value over 130 hours, and maintained this output even after 800 hours. Then the power density-voltage relationship of the cell was measured by changing inserted variable resistance from 1 KΩ to 2.2 MΩ, which is showed in Figure 6(c). The maximum power density was 0.29 μW/cm^2 (1.52 uA/cm^2) at 0.19 V. The cell prototype showed stable output over several hundred hours.

We have also tried to use the PPy film/Au as the anode of the cell prototype. However, the cell output decreased quickly with the time, and reached zero within 10 hours. The poor performance of the cell prototype might be ascribed to the structure of PPy film. More research is needed to investigate the difference in the structure between PPy inverse opal and PPy film. In addition, the research will also focus on the improvement of the performance of the cell, developing PPy anode-based cell for practical use.

4. Conclusion

In this paper, we developed a cell prototype which can operate in a physiological buffer. The anode of the cell is

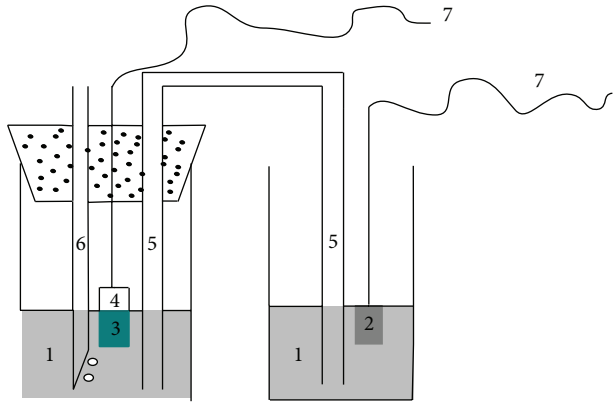

Figure 5: Schematic view of the cell prototype with PPy inverse opal/Au anode and Pt plate cathode. (1) 0.1 M PBS of pH 7.0; (2) Pt plate cathode with the area of 12 mm^2; (3) PPy inverse opal/Au; (4) insulating tape covered on the gold substrate; (5) KCl salt bridge; (6) gas supply pipe; and (7) conducting wire.

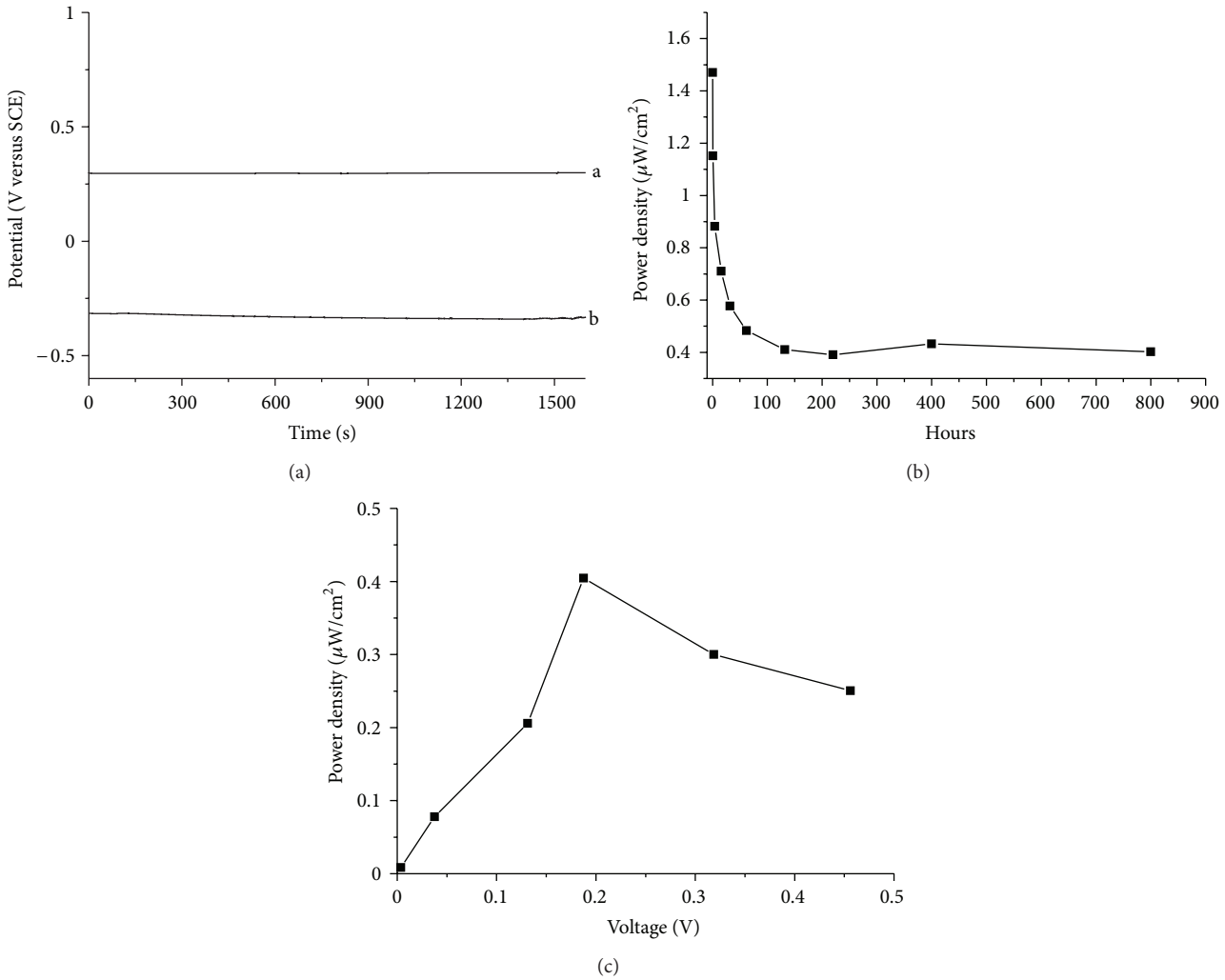

Figure 6: (A) The OCP-time curve of Pt plate electrode in 0.1 M PBS of pH 7.0 in the air (a), and the OCP-time curve of PPy inverse opal/Au in N_2-saturated PBS of pH 7.0 (b); (B) performance evaluation of the cell: Time evolutions of the cell output measured with 200 KΩ load; (C) power density versus voltage measured by changing the load from 1 KΩ to 2.2 MΩ.

a gold substrate modified with a PPy inverse opaline film, which was fabricated by electropolymerization of pyrrole in an acetonitrile solution containing both [bmim]PF_6 and pyrrole monomer through cyclic voltammetry technique. The electrical energy of the PPy inverse opal/Au came from the attack of radical cationic centers the PPy inverse opal by OH^- groups. Although the performance evaluation suggested that the cell show stable output over several hundred hours, the power density need to be improved further for practical application, which will be our next research.

Acknowledgments

The authors acknowledge the supports of National Natural Science Foundation of China (11074087, 21001072, 21102088, and 21174081); the Program for Professor of Special Appointment (Eastern Scholar) at Shanghai Institutions of Higher Learning; Key subject of Shanghai Municipal Education Commission (J50102); and Shanghai Leading Academic Discipline Project (S30107).

References

[1] J. M. Pringle, J. Efthimiadis, P. C. Howlett et al., "Electrochemical synthesis of polypyrrole in ionic liquids," *Polymer*, vol. 45, no. 5, pp. 1447–1453, 2004.

[2] S. Komaba, M. Seyama, T. Momma, and T. Osaka, "Potentiometric biosensor for urea based on electropolymerized electroinactive polypyrrole," *Electrochimica Acta*, vol. 42, no. 3, pp. 383–388, 1997.

[3] T. Welton, "Room-temperature ionic liquids. Solvents for synthesis and catalysis," *Chemical Reviews*, vol. 99, no. 8, pp. 2071–2083, 1999.

[4] S. R. Yun, G. O. Kim, C. W. Lee, N. J. Jo, Y. Kang, and K. S. Ryu, "Synthesis and control of the shell thickness of polyaniline and polypyrrole half hollow spheres using the polystyrene cores," *Journal of Nanomaterials*, vol. 2012, Article ID 894539, 9 pages, 2012.

[5] M. Deepa and S. Ahmad, "Polypyrrole films electropolymerized from ionic liquids and in a traditional liquid electrolyte: a comparison of morphology and electro-optical properties," *European Polymer Journal*, vol. 44, no. 10, pp. 3288–3299, 2008.

[6] K. Sekiguchi, M. Atobe, and T. Fuchigami, "Electropolymerization of pyrrole in 1-ethyl-3-methylimidazolium trifluoromethanesulfonate room temperature ionic liquid," *Electrochemistry Communications*, vol. 4, no. 11, pp. 881–885, 2002.

[7] A. Zhang, J. Chen, D. Niu, G. G. Wallace, and J. Lu, "Electrochemical polymerization of pyrrole in $BMIMPF_6$ ionic liquid and its electrochemical response to dopamine in the presence of ascorbic acid," *Synthetic Metals*, vol. 159, no. 15-16, pp. 1542–1545, 2009.

[8] W. Lu, A. G. Fadeev, B. Qi et al., "Use of ionic liquids for π-conjugated polymer electrochemical devices," *Science*, vol. 297, no. 5583, pp. 983–987, 2002.

[9] T. Cassagneau and F. Caruso, "Inverse opals for optical affinity biosensing," *Advanced Materials*, vol. 14, no. 22, pp. 1629–1633, 2002.

[10] T. Cassagneau and F. Caruso, "Conjugated polymer inverse opals for potentiometric biosensing," *Advanced Materials*, vol. 14, no. 24, pp. 1837–1841, 2002.

[11] Y. Wang and F. Caruso, "Enzyme encapsulation in nanoporous silica spheres," *Chemical Communications*, vol. 10, no. 13, pp. 1528–1529, 2004.

[12] Y. Wang and F. Caruso, "Macroporous zeolitic membrane bioreactors," *Advanced Functional Materials*, vol. 14, no. 10, pp. 1012–1018, 2004.

[13] W. Qian, Z. Z. Gu, A. Fujishima, and O. Sato, "Three-dimensionally ordered macroporous polymer materials: an approach for biosensor applications," *Langmuir*, vol. 18, no. 11, pp. 4526–4529, 2002.

[14] P. V. Braun and P. Wiltzius, "Electrochemically grown photonic crystals," *Nature*, vol. 402, no. 6762, pp. 603–604, 1999.

[15] P. Jiang, J. Cizeron, J. F. Bertone, and V. L. Colvin, "Preparation of macroporous metal films from colloidal crystals," *Journal of the American Chemical Society*, vol. 121, no. 34, pp. 7957–7958, 1999.

[16] L. Xu, W. L. Zhou, C. Frommen et al., "Electrodeposited nickel and gold nanoscale metal meshes with potentially interesting photonic properties," *Chemical Communications*, no. 12, pp. 997–998, 2000.

[17] P. N. Bartlett, P. R. Birkin, and M. A. Ghanem, "Electrochemical deposition of macroporous platinum, palladium and cobalt films using polystyrene latex sphere templates," *Chemical Communications*, no. 17, pp. 1671–1672, 2000.

[18] P. N. Bartlett, J. J. Baumberg, P. R. Birkin, M. A. Ghanem, and M. C. Netti, "Highly ordered macroporous gold and platinum films formed by electrochemical deposition through templates assembled from submicron diameter monodisperse polystyrene spheres," *Chemistry of Materials*, vol. 14, no. 5, pp. 2199–2208, 2002.

[19] X. Chen, Y. Wang, J. Zhou, W. Yan, X. Li, and J. J. Zhu, "Electrochemical impedance immunosensor based on three-dimensionally ordered macroporous gold film," *Analytical Chemistry*, vol. 80, no. 6, pp. 2133–2140, 2008.

[20] T. Cassagneau and F. Caruso, "Semiconducting polymer inverse opals prepared by electropolymerization," *Advanced Materials*, vol. 14, no. 1, pp. 34–38, 2002.

[21] D. Wang and F. Caruso, "Fabrication of polyaniline inverse opals via templating ordered colloidal assemblies," *Advanced Materials*, vol. 13, no. 5, pp. 350–354, 2001.

[22] S. Tian, J. Wang, U. Jonas, and W. Knoll, "Inverse opals of polyaniline and its copolymers prepared by electrochemical techniques," *Chemistry of Materials*, vol. 17, no. 23, pp. 5726–5730, 2005.

[23] E. Yablonovitch, "Inhibited spontaneous emission in solid-state physics and electronics," *Physical Review Letters*, vol. 58, no. 20, pp. 2059–2062, 1987.

[24] S. Kubo, Z. Z. Gu, K. Takahashi, Y. Ohko, O. Sato, and A. Fujishima, "Control of the optical band structure of liquid crystal infiltrated inverse opal by a photoinduced nematic-isotropic phase transition," *Journal of the American Chemical Society*, vol. 124, no. 37, pp. 10950–10951, 2002.

[25] A. Saheb, J. Janata, and M. Josowicz, "Reference electrode for ionic liquids," *Electroanalysis*, vol. 18, no. 4, pp. 405–409, 2006.

[26] S. Wong, V. Kitaev, and G. A. Ozin, "Colloidal crystal films: advances in universality and perfection," *Journal of the American Chemical Society*, vol. 125, no. 50, pp. 15589–15598, 2003.

[27] Z. Zhou and X. S. Zhao, "Flow-controlled vertical deposition method for the fabrication of photonic crystals," *Langmuir*, vol. 20, no. 4, pp. 1524–1526, 2004.

[28] M. Yoldi, C. Arcos, B. R. Paulke, R. Sirera, W. González-Viñas, and E. Görnitz, "On the parameters influencing the deposition of polystyrene colloidal crystals," *Materials Science and Engineering C*, vol. 28, no. 7, pp. 1038–1043, 2008.

[29] L. Zhao, L. Tong, C. Li, Z. Gu, and G. Shi, "Polypyrrole actuators with inverse opal structures," *Journal of Materials Chemistry*, vol. 19, no. 11, pp. 1653–1658, 2009.

[30] M. Zhou and J. Heinze, "Electropolymerization of pyrrole and electrochemical study of polypyrrole. 3. Nature of "water effect" in acetonitrile," *Journal of Physical Chemistry B*, vol. 103, no. 40, pp. 8451–8457, 1999.

[31] M. Zhou and J. Heinze, "Electropolymerization of pyrrole and electrochemical study of polypyrrole. 2. influence of acidity on the formation of polypyrrole and the multipathway mechanism," *Journal of Physical Chemistry B*, vol. 103, no. 40, pp. 8443–8450, 1999.

[32] M. Zhou and J. Heinze, "Electropolymerization of pyrrole and electrochemical study of polypyrrole: 1. Evidence for structural diversity of polypyrrole," *Electrochimica Acta*, vol. 44, no. 11, pp. 1733–1748, 1999.

[33] M. Zhou, M. Pagels, B. Geschke, and J. Heinze, "Electropolymerization of pyrrole and electrochemical study of polypyrrole. 5. Controlled electrochemical synthesis and solid-state transition of well-defined polypyrrole variants," *Journal of Physical Chemistry B*, vol. 106, no. 39, pp. 10065–10073, 2002.

[34] S. Sowmiah, V. Srinivasadesikan, M. C. Tseng, and Y. H. Chu, "On the chemical stabilities of ionic liquids," *Molecules*, vol. 14, no. 9, pp. 3780–3813, 2009.

[35] W. L. Dai, M. H. Qiao, and J. F. Deng, "XPS studies on a novel amorphous Ni-Co-W-B alloy powder," *Applied Surface Science*, vol. 120, no. 1-2, pp. 119–124, 1997.

[36] F. Beck and R. Michaelis, "Corrosion of synthetic metals," *Werkstoffe und Korrosion*, vol. 42, no. 7, pp. 341–347, 1991.

[37] F. Beck, U. Barsch, and R. Michaelis, "Corrosion of conducting polymers in aqueous media," *Journal of Electroanalytical Chemistry*, vol. 351, no. 1-2, pp. 169–184, 1993.